Dalton Transactions

PAPER

View Article Online
View Journal | View Issue

Cite this: *Dalton Trans.*, 2019, **48**, 10464

Novel latonduine derived proligands and their copper(II) complexes show cytotoxicity in the nanomolar range in human colon adenocarcinoma cells and *in vitro* cancer selectivity†

Felix Bacher,*[a] Christopher Wittmann,[a] Márta Nové,[b] Gabriella Spengler,[b] Małgorzata A. Marć,[c] Eva A. Enyedy,[c] Denisa Darvasiová,[d] Peter Rapta,[d] Thomas Reiner[e,f,g] and Vladimir B. Arion*[a]

Received 22nd March 2019,
Accepted 10th May 2019

DOI: 10.1039/c9dt01238a

rsc.li/dalton

Four Schiff bases derived from 7-hydrazin-yl-5,8-dihydroindolo[2,3-*d*][2]benzazepin-(6*H*)-one and its bromo-substituted analogue (HL^1–HL^4) and four copper(II) complexes **1–4** have been synthesised and fully characterised by standard spectroscopic methods (^{1}H and ^{13}C NMR, UV-vis), ESI mass spectrometry, single crystal X-ray diffraction and spectroelectrochemistry. In addition, two previously reported complexes with paullone ligands **5** and **6** were prepared and studied for comparison reasons. The Cu^{II} ion in **1–4** is five-coordinate and adopts a square-pyramidal or slightly distorted square-pyramidal coordination geometry. The ligands HL^{1-4} act as tridentate, the other two coordination places are occupied by two chlorido co-ligands. The organic ligands in **2** and **3** are bound tighter to copper(II) when compared to related paullone ligands in **5** and **6**. The new compounds show very strong cytotoxic activity against human colon adenocarcinoma doxorubicin-sensitive Colo 205 and multidrug resistant Colo 320 cancer cell lines with IC_{50} values in the low micromolar to nanomolar concentration range.

Introduction

Indolobenzazepines are a class of compounds with a broad spectrum of biological activities, amongst them analgesic, antidepressant, antimalarial, antidiabetic, anticancer and antiparasitic.[1–7] The search for potent kinase inhibitors led to indolo[3,2-*d*]benzazepines, known as paullones.[8] Cyclin dependent kinases (cdks) are attractive targets for anticancer drugs, since they control the cell cycle.[9] Research on structure–activity relationships (SARs) showed that electron-withdrawing groups in position 9 of the paullone scaffold (Chart 1, left) enhance the cdk inhibition, while the lactam moiety is essential for the anticancer activity. This finding resulted in the discovery of the lead compounds kenpaullone and alsterpaullone (Chart 1).[10] Despite their potency, paullones possess some adverse properties. In particular, the low aqueous solubility and bio-

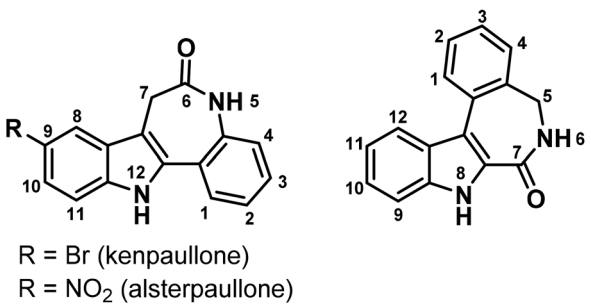

Chart 1 The indolo[3,2-*d*]benzazepine (paullone) (left), *vs.* the indolo[2,3-*d*]benzazepine backbone (right) with numbering schemes.

[a]*Institute of Inorganic Chemistry of the University of Vienna, Währinger Strasse 42, A-1090 Vienna, Austria. E-mail: felix.bacher@univie.ac.at, vladimir.arion@univie.ac.at*
[b]*Department of Medical Microbiology and Immunobiology, University of Szeged, Dóm tér 10, H-6720 Szeged, Hungary*
[c]*Department of Inorganic and Analytical Chemistry, Interdisciplinary Excellence Centre, University of Szeged, Dóm tér 7, H-6720 Szeged, Hungary*
[d]*Institute of Physical Chemistry and Chemical Physics, Slovak University of Technology in Bratislava, Radlinského 9, 81237 Bratislava, Slovak Republic*
[e]*Department of Radiology, Weill Cornell Medical College, New York City, NY 10065, USA*
[f]*Department of Radiology, Memorial Sloan Kettering Cancer Center, New York City, NY 10065, USA*
[g]*Chemical Biology Program, Memorial Sloan Kettering Cancer Center, New York City, NY 10065, USA*

†Electronic supplementary information (ESI) available: NMR numbering scheme for HL^1–HL^4 (Scheme S1), synthesis of **B** (Scheme S2), cyclic voltammograms of **2** and **3** (Fig. S1), UV-vis-NIR spectroelectrochemistry for **3** (Fig. S2), NMR spectra (Fig. S3–S20), ESI-MS spectra (Fig. S21–S32). CCDC 1903184–1903189. For ESI and crystallographic data in CIF or other electronic format see DOI: 10.1039/c9dt01238a

availability hampered their clinical use. Later it was shown that the bioavailability can be improved by the attachment of suitable metal binding sites onto the paullone backbone and the consequent metal complex formation with gallium(III), ruthenium(II), osmium(II) and copper(II) ions. This led to highly cytotoxic compounds with an enhanced aqueous solubility, with copper(II) complexes being the most active ones.[11–16] However, cdks seem not to be the main target for these metal complexes.[17] Alternative mechanisms of action have been suggested, amongst them DNA intercalation.[14]

In our present work, we focused our attention on the isomeric indolo[2,3-*d*]benzazepine scaffold (Chart 1, right). It differs from the paullone core by the position of the lactam group in the azepine ring and features a flipped indole moiety with respect to the benzazepinone half of the molecule. These new compounds contain a typical latonduine structural motif. Latonduine-modified molecules usually exhibit prominent anticancer activity *in vitro*, along with the ability to inhibit tubulin polymerisation.[18–21] Like paullones, these compounds do not possess any metal binding site. Therefore, it was of interest to us to chemically modify them and obtain proligands with potentially tridentate κN, $\kappa N'$, $\kappa N''$ metal binding site, in particular, for copper(II). Copper is an essential trace metal and therefore considered to be safer than other metals used in chemotherapy, *e.g.* platinum.[22,23] In addition, it is well-established that copper(II) is able to strongly enhance the cytotoxicity of biologically active ligands.[24]

Herein we report on the synthesis and characterisation of four novel latonduine core containing proligands and their copper(II) complexes. In order to obtain structure–activity relationships we modified the indolobenzazepine backbone by inserting a bromine substituent at position 11, the equivalent to position 9 in the paullone scaffold (compare kenpaullone). In addition, an aldehyde and a ketone containing a functional group in a position suitable for chelate formation were used for Schiff base condensation reactions, namely 2-formyl- and 2-acetylpyridine (Chart 2).

The new compounds have been characterised by ^{1}H and ^{13}C NMR spectroscopy (**HL^{1}**–**HL^{4}**), single crystal X-ray diffraction (**HL^{4}**, **1**–**4**) and ESI mass spectrometry; their purity was validated by elemental analysis. Solution equilibrium properties of **HL^{3}** and its copper(II) complex **3** were characterised in a DMSO–water solvent mixture by UV-vis titrations. The cytotoxicity of the proligands and the corresponding copper(II) complexes was tested in Colo 205 (chemosensitive) and Colo 320/MDR-LRP (multidrug resistant) human colon adenocarcinoma cell lines and one non-cancerous human embryonal lung fibroblast MRC-5 cell line and compared to those of the two previously reported paullone-derived copper(II) complexes **5** and **6** (Chart 3).[15,25] The new compounds showed very high activity with IC_{50} values from the low micromolar to the nanomolar concentration range and were superior to **5** and **6** in cancer cell lines, while less cytotoxic in non-cancerous MRC-5 cells. Furthermore some selectivity for cancer cells over normal cells was observed in most cases, making this compound class pertinent for further development as anticancer drugs.

Experimental

2-Iodobenzonitrile, ethyl-1*H*-indole-carboxylate and 5-bromo-ethyl-1*H*-indole-carboxylate were purchased from ABCR. Borane solution (1 M in THF), absolute DMF, dimethylaminopyridine, di-*tert*-butyl-dicarbonate, absolute acetonitrile, palladium(II) acetate, sodium bicarbonate, basic aluminium oxide, 2-acetylpyridine and 2-formylpyridine were bought from Fisher/Acros Organics. Ethoxy-methylchloride was obtained form TCI. Sodium hydride, phosphorus(V) sulfide, celite, hydrazine monohydrate and methyl iodide were purchased from Sigma Aldrich, while lithium hydroxide monohydrate and triphenylphosphine were from Alfa Aesar. 1-Ethyl-3-(3-dimethylaminopropyl)carbodiimide-hydrochloride was purchased from IRIS biotech, while silver(I) carbonate from Merck. 2-Iodobenzylamine was prepared by a known method.[26] The unsubstituted indolo[2,3-*d*]benzazepine (**A**) was prepared by following published protocols.[18–20] The 11-bromo-substituted species **B** was prepared using reported procedures,[18–20] with some modifications. A detailed description of the synthesis of **B** is given in the ESI.†

Synthesis of proligands

5,8-Dihydroindolo[2,3-*d*][2]benzazepin-7(6*H*)-thione (C). 5,8-Dihydroindolo[2,3-*d*][2]benzazepin-7(6*H*)-one (**A**) (966 mg, 3.88 mmol) was dissolved in absolute acetonitrile (77 mL) in a Schlenk tube under argon atmosphere. A mixture of phosphorus(V) pentasulfide and basic aluminium oxide (0.6 : 1 w/w)[27] (1.60 g) was added and the reaction mixture was stirred at 85 °C overnight. The next day, the mixture was cooled to room temperature and filtered. The filtrate was concentrated *in vacuo* and taken up in water (50 mL). The pH was adjusted to 8 using saturated potassium carbonate solution. The solution was extracted with dichloromethane (DCM) (3 × 100 mL). The organic phases were combined and dried over magnesium sulfate. The dried organic phase was concentrated and the raw product was purified on silica using a mixture of DCM : methanol 99 : 1 as eluent. Yield: 841 mg, 82%. ^{1}H NMR (500 MHz, DMSO-d_6) δ 11.78 (s, 1H, N*H*), 10.57 (t, J = 5.5 Hz, 1H, N*H*), 7.98 (dd, J = 14.4, 7.9 Hz, 2H, $H_{(Ar)}$), 7.64 (d, J = 8.3 Hz, 1H, $H_{(Ar)}$), 7.53 (t, J = 7.5 Hz, 1H, $H_{(Ar)}$), 7.48 (d, J = 6.9 Hz, 1H, $H_{(Ar)}$), 7.41 (t, J = 7.3 Hz, 1H, $H_{(Ar)}$), 7.36 (t, J = 7.4 Hz, 1H, $H_{(Ar)}$), 7.20 (t, J = 7.5 Hz, 1H, $H_{(Ar)}$), 4.41–4.28 (m, 1H, CH_2), 4.04 (d, J = 12.2 Hz, 1H, CH_2). ESI-MS (acetonitrile/methanol + 1% water), positive: m/z 265.08 $[M + H]^+$.

11-Bromo-5,8-dihydroindolo[2,3-*d*][2]benzazepin-7(6*H*)-thione (D). 5,8-Dihydroindolo[2,3-*d*][2]benzazepin-7(6*H*)-one (**B**) (1.00 g, 3.06 mmol) and a mixture of phosphorus(V) pentasulfide and basic aluminium oxide (0.6 : 1 w/w)[27] (2.20 g) were suspended in dry THF (50 mL) in an 100 mL Schlenk tube, under argon atmosphere. The reaction mixture was stirred overnight at 75 °C. The next day it was cooled to room temperature, the yellow precipitate was filtered off and washed with THF. The filtrate was evaporated and the residue was purified on silica by using DCM/methanol 99 : 1 as eluent. The product was obtained as yellow-orange powder after removal of the solvent. Yield: 635 mg, 60%. ^{1}H NMR (500 MHz, DMSO-d_6)

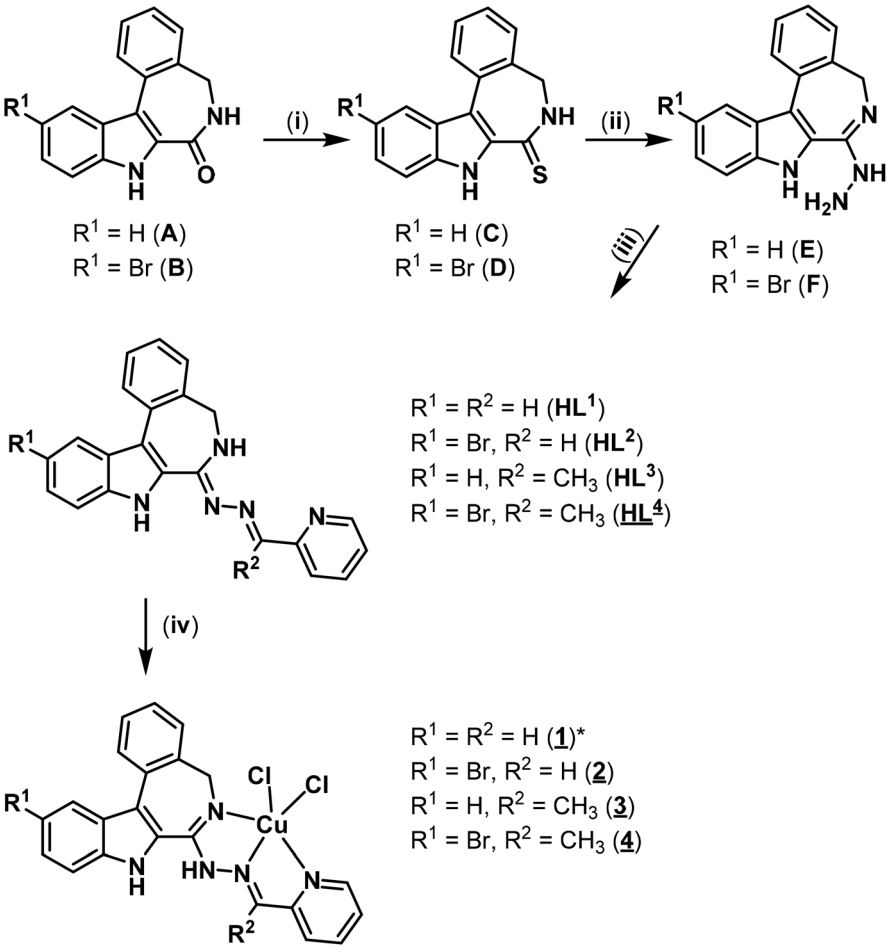

Chart 2 New proligands and copper(II) complexes synthesised in this work.[a] Underlined numbers indicate compounds studied by X-ray diffraction. ***1** crystallised from DMF as the trimer $[Cu_3Cl_4(HL^1)_3]Cl_2$ (1^{trim}). [a]Reagents and conditions: (i) **C**: phosphorus pentasulfide/aluminium oxide, acetonitrile, 85 °C, overnight; **D**: phosphorus pentasulfide/aluminium oxide, tetrahydrofuran, 75 °C, overnight; (ii) hydrazine monohydrate, reflux, overnight; (iii) HL^1, HL^2: 2-formypyridine, ethanol, 85 °C, overnight; HL^3, HL^4: 2-acetylpyridine, ethanol, 85 °C, overnight; (iv) $CuCl_2{\cdot}2H_2O$, isopropanol, reflux, 15 min.

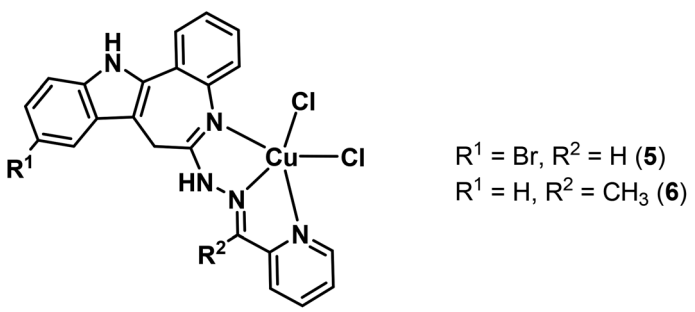

Chart 3 Paullone-derived copper(II) complexes used in this study.[15,25]

δ 12.00 (s, 1H, N*H*), 10.67 (t, J = 5.6 Hz, 1H, N*H*), 8.10 (d, J = 1.7 Hz, 1H, $H_{(Ar)}$), 7.93 (d, J = 7.2 Hz, 1H, $H_{(Ar)}$), 7.60 (d, J = 8.7 Hz, 1H, $H_{(Ar)}$), 7.55 (td, J = 7.5, 1.4 Hz, 1H, $H_{(Ar)}$), 7.51–7.47 (m, 2H, $H_{(Ar)}$), 7.43 (td, J = 7.4, 1.1 Hz, 1H, $H_{(Ar)}$), 4.33 (s, 1H, CH_2), 4.06 (d, J = 12.5 Hz, 1H, CH_2). ESI-MS (acetonitrile/methanol + 1% water), positive, m/z 344.99 $[M + H]^+$.

7-Hydrazin-yl-5,8-dihydroindolo[2,3-*d*][2]benzazepin-(6*H*)-one (E). A suspension of 5,8-dihydroindolo[2,3-*d*][2]benzazepin-7(6*H*)-thione (**C**) (582 mg, 2.21 mmol) in hydrazine monohydrate (8 mL) under argon atmosphere was refluxed overnight. On the next day the reaction mixture was cooled to room temperature and the pale yellow precipitate was filtered off, washed

with water and dried *in vacuo*. Yield: 496 mg, 86%. ^{1}H NMR (500 MHz, DMSO-d_6) δ 11.43 (s, 1H, N*H*), 7.86 (t, J = 8.5 Hz, 2H, $H_{(Ar)}$), 7.49–7.40 (m, 2H, $H_{(Ar)}$), 7.37 (d, J = 6.5 Hz, 1H), $H_{(Ar)}$, 7.20 (dt, J = 21.5, 7.3 Hz, 2H, $H_{(Ar)}$), 7.09 (t, J = 7.0 Hz, 1H, $H_{(Ar)}$), 6.32 (s, 1H, N*H*), 5.00 (s, 2H, NH_2), 4.07 (s, 2H, CH_2). ESI-MS (acetonitrile/methanol + 1% water), positive: m/z 263.09 $[M + H]^+$.

11-Bromo-7-hydrazin-yl-5,8-dihydroindolo[2,3-*d*][2]benzazepin-(6*H*)-one (F). A suspension of 11-bromo-5,8-dihydroindolo[2,3-*d*][2]benzazepin-7(6*H*)-thione (**D**) (830 mg, 2.42 mmol) in hydrazine monohydrate (20 mL) under argon atmosphere was refluxed overnight. On the next day the reaction mixture was cooled to room temperature and the pale yellow precipitate was filtered off, washed with water and dried *in vacuo*. Yield: 757 mg, 92%. 1H NMR (500 MHz, DMSO-d_6) δ 7.97 (d, J = 1.8 Hz, 1H, $H_{(Ar)}$), 7.80 (d, J = 7.2 Hz, 1H, $H_{(Ar)}$), 7.47–7.37 (m, 3H, $H_{(Ar)}$), 7.33–7.29 (m, 1H, $H_{(Ar)}$), 7.25 (td, J = 7.4, 1.0 Hz, 1H, $H_{(Ar)}$), 6.36 (s, 1H, N*H*), 5.07 (s, 2H, NH_2), 4.06 (s, 2H, CH_2). ESI-MS (acetonitrile/methanol + 1% water), positive: m/z 343.24 $[M + H]^+$.

HL^1·0.4C$_2$H$_5$OH. A solution of 7-hydrazin-yl-5,8-dihydroindolo[2,3-*d*][2]benzazepin-(6*H*)-one (**E**) (199 mg, 0.76 mmol) in ethanol (3 mL) in a 25 mL Schlenk tube was degassed by bubbling argon through the solution for 10 min. 2-Formylpyridine (79 μL, 0.83 mmol) was added and the mixture was stirred overnight at 85 °C. The next day the reaction mixture was cooled to room temperature and the solvent was evaporated. The residue was taken up in water (10 mL) and ethanol was added until complete dissolution. Then, the solvent was removed slowly under reduced pressure until precipitation started. The mixture was allowed to stand at 4 °C overnight. The next day, a yellow precipitate was filtered off, washed with water/ethanol 2 : 1 and dried *in vacuo*. Yield: 266 mg, 99%. Anal. Calcd for $C_{22}H_{17}N_5$·0.4C_2H_5OH (M 372.13 g mol^{-1}): C, 73.71; H, 5.07, N, 19.09. Found: C, 73.91; H, 5.33; N, 18.82. ^{1}H NMR (600 MHz, DMSO-d_6) δ 11.93 (s, 1H, H^{12}), 8.59 (d, J = 4.1 Hz, 1H, H^{18}), 8.37 (d, J = 8.0 Hz, 2H, H^{15}, H^{21}), 8.31 (t, J = 5.4 Hz, 1H, H^6), 7.98 (dd, J = 15.4, 7.6 Hz, 2H, H^{12}, H^3), 7.87 (td, J = 7.5, 1.2 Hz, 1H, H^{20}), 7.60 (d, J = 8.2 Hz, 1H, H^9), 7.53–7.49 (m, 1H, H^2), 7.47 (d, J = 6.6 Hz, 1H, H^4), 7.40–7.31 (m, 3H, H^{10}, H^1, H^{19}), 7.20 (dd, J = 11.1, 4.0 Hz, 1H, H^{11}), 4.36–4.02 (m, 2H, H^5). ^{13}C NMR (151 MHz, DMSO) δ 155.62 (Cq, C^7), 154.52 (Cq, C^{16}), 152.14 (CH, C^{15}), 149.28 (CH, C^{18}), 137.78 (Cq, C^{4a}), 136.76 (Cq, C^{8a}), 136.30 (CH, C^{20}), 133.161 (Cq, C^{12c}), 129.01(Cq, C^{7a}), 128.09 (CH, C^4), 128.06 (CH, C^2), 127.41 (CH, C^3), 126.33 (CH, C^1), 124.94 (Cq, C^{12a}), 124.10(CH, C^{10}), 123.87 (CH, C^{19}), 120.77 (CH, C^{21}), 120.46 (CH, C^{11}), 120.22 (CH, C^{12}), 117.12(Cq, C^{12b}), 112.69(CH, C^9), 46.00 (CH^2, C^5). For atom numbering scheme see ESI, Scheme S1.† ESI-MS (acetonitrile/methanol + 1% water), positive: m/z 352.26 $[M + H]^+$.

HL^2·H$_2$O. A solution of 11-bromo-7-hydrazin-yl-5,8-dihydroindolo[2,3-*d*][2]benzazepin(6*H*)one (**F**) (370 mg, 1.08 mmol) in ethanol (6 mL) in a 25 mL Schlenk tube was degassed by bubbling argon through the solution for 10 min. 2-Formylpyridine (113 μL, 1.19 mmol) was added and the mixture was stirred overnight at 85 °C. The next day the reaction mixture was cooled to room temperature and the solvent was removed under reduced pressure. The residue was dissolved in methanol (10 mL). This solution was concentrated under reduced pressure to about half the volume, when the formation of a yellow precipitate was observed. The resulting suspension was allowed to stand at 4 °C overnight. On the next day the precipitate was filtered off and washed with cold methanol. Yield: 135 mg, 31%. Anal. Calcd for $C_{22}H_{16}BrN_5$·H_2O (M 448.32 g mol^{-1}): C, 58.93; H, 4.05, N, 15.62. Found: C, 58.86; H, 3.97; N, 15.67. ^{1}H NMR (700 MHz, DMSO-d_6) δ 12.14 (s, 1H, H^8), 8.59 (d, J = 4.6 Hz, 1H, H^{18}), 8.38–8.35 (m, 2H, H^{15}, H^{21}), 8.32 (t, J = 5.3 Hz, 1H, H^6), 8.10 (d, J = 1.5 Hz, 1H, H^{12}), 7.92 (d, J = 7.6 Hz, 1H, H^1), 7.86 (dd, J = 11.0, 4.4 Hz, 1H, H^{20}), 7.56 (d, J = 8.7 Hz, 1H, H^9), 7.52 (t, J = 7.5 Hz, 1H, H^2), 7.47–7.44 (m, 2H, H^{10}, H^4), 7.39–7.34 (m, 2H, H^{19}, H^3), 4.46–3.99 (m, 2H, H^5). ^{13}C NMR (176 MHz, DMSO-d_6) δ 155.25 (Cq, C^7), 154.40 (Cq, C^{16}), 152.52 (CH, C^{15}), 149.29 (CH, C^{18}), 137.86 (Cq, C^{4a}), 136.30 (CH, C^{20}), 135.39 (Cq, C^{8a}), 132.95 (Cq, C^{12}), 130.29 (Cq, C^{7a}), 128.27 (CH, C^4), 128.17 (CH, C^2), 127.35 (CH, C^1), 126.71 (CH, C^{10}), 126.63 (CH, C^3), 126.54 (Cq, C^{12a}), 123.95 (CH, C^{19}), 122.23 (CH, C^{12}), 120.82 (CH, C^{21}), 116.48 (Cq, C^{12b}), 114.70 (CH, C^9), 113.01 (Cq, C^{11}), 45.91 (CH$_2$, C^5). For atom numbering scheme see ESI, Scheme S1.† ESI-MS (acetonitrile/methanol + 1% water), positive: m/z 432.06 $[M + H]^+$.

HL^3. A solution of 7-hydrazin-yl-5,8-dihydroindolo[2,3-*d*][2]benzazepin(6*H*)one (**E**) (200 mg, 0.76 mmol) in ethanol (3.5 mL) in a 25 mL Schlenk tube was degassed by bubbling argon through the solution for 10 min. 2-Acetylpyridine (94 μL, 0.84 mmol) was added and the mixture was stirred overnight at 86 °C. The next day the reaction mixture was cooled to room temperature and stored at 4 °C for 2 h. The yellow precipitate was filtered off and washed with cold ethanol. Yield: 261 mg, 94%. Anal. Calcd for $C_{23}H_{19}N_5$ (M 365.43 g mol^{-1}): C, 75.59; H, 5.24, N, 19.16. Found: C, 75.32; H, 5.05; N, 19.00. ^{1}H NMR (600 MHz, DMSO-d_6) δ 11.77 (s, 1H, H^8), 8.62–8.55 (m, 1H, H^{18}), 8.50 (d, J = 8.0 Hz, 1H^2), 8.02–7.91 (m, 3H, H^1, H^5, H^{12}), 7.81 (td, J = 7.8, 1.8 Hz, 1H, H^{20}), 7.62 (d, J = 8.2 Hz, 1H, H^9), 7.49 (td, J = 7.6, 1.2 Hz, 1H, H^2), 7.43 (d, J = 6.8 Hz, 1H, H^4), 7.40–7.29 (m, 3H, H^3, H^{19}, H^{10}), 7.19 (dt, J = 18.3, 5.5 Hz, 1H, H^{11}), 4.64–3.75 (m, 2H, H^5), 2.50 (s, 3H, H^{22} (overlapped DMSO signal)). ^{13}C NMR (151 MHz, DMSO-d_6) δ 158.23 (Cq, C^{15}), 156.45 (Cq, C^{16}), 153.36 (Cq, C^7), 148.44 (CH, C^{18}), 137.95 (Cq, C^{4a}), 136.65 (Cq, C^{8a}), 135.88 (CH, C^{20}), 133.74 (Cq, C^{12c}), 129.75 (Cq, C^{7a}), 128.07 (CH, C^4), 127.97 (CH, C^2), 127.33 (CH, C^1), 126.18 (CH, C^3), 125.05 (Cq, C^{12a}), 123.92 (CH, C^{10}), 123.52 (CH, C^{19}), 120.84 (CH, C^{21}), 120.37 (CH, C^{11}), 120.13 (CH, C^{12}), 116.50 (Cq, C^{12b}), 112.62 (CH, C^9), 45.97 (CH$_2$, C^5) 13.08 (CH$_3$, C^{22}). For atom numbering scheme see ESI†, Scheme S1.† ESI-MS (acetonitrile/methanol + 1% water), positive: m/z 366.16 $[M + H]^+$.

HL^4. A solution of 11-bromo-7-hydrazin-yl-5,8-dihydroindolo [2,3-*d*][2]benzazepin(6*H*)one (**F**) (76 mg, 0.22 mmol) in ethanol (2 mL) in a 10 mL Schlenk tube was degassed by bubbling argon through the solution for 10 min. 2-Acetylpyridine (27 μL, 0.24 mmol) was added and the mixture was stirred overnight at 85 °C. The next day the reaction mixture was cooled to room temperature and allowed to stand at 4 °C for

2 days. The yellow-brown plates of X-ray diffraction quality were filtered off and washed with cold ethanol. Yield: 57 mg, 58%. Anal. Calcd for $C_{23}H_{18}BrN_5$ (M 444.33 g mol^{-1}): C, 62.17; H, 4.08, N, 15.76. Found: C, 61.86; H, 4.13; N, 15.74. ^{1}H NMR (600 MHz, DMSO-d_6) δ 11.98 (s, 1H, H^8), 8.60–8.56 (m, 1H, H^{18}), 8.53–8.44 (m, 1H, H^{21}), 8.09 (d, J = 1.8 Hz, 1H, H^{12}), 7.99 (t, J = 5.3 Hz, 1H, H^6), 7.93–7.90 (m, 1H, H^1), 7.82 (ddd, J = 8.0, 7.5, 1.8 Hz, 1H, H^{20}), 7.58 (d, J = 8.7 Hz, 1H, H^9), 7.54–7.49 (m, 1H, H^2), 7.47–7.42 (m, 2H, H^{10}, H^4), 7.38–7.33 (m, 2H, H^{19}, H^3), 4.39–4.08 (m, 2H, H^5), 2.49 (s, 3H, H^{22} (overlapped DMSO signal)). ^{13}C NMR (151 MHz, DMSO-d_6) δ 158.62 (Cq, C^{15}), 156.34 (Cq, C^{16}), 152.96 (Cq, C^7), 148.45 (CH, C^{18}), 138.04 (Cq, C^{4a}), 135.91 (CH, C^{20}), 135.30 (Cq, C^{8a}), 133.08 (Cq, C^{12c}), 131.02 (Cq, C^{7a}), 128.20 (CH, C^4), 128.15 (CH, C^2), 127.28 (CH, C^1), 126.68 (Cq, C^{12a}), 126.53 (CH, C^{10}), 126.49 (CH, C^{19}), 123.61 (CH, C^3), 122.14 (CH, C^{12}), 120.88 (CH, C^{21}), 115.90 (Cq, C^{12b}), 114.65 (CH, C^9), 112.92 (Cq, C^{11}), 45.88 (CH_2, C_5), 13.10 (CH_3, C^{22}). For atom numbering scheme see ESI, Scheme S1.† ESI-MS (acetonitrile/methanol + 1% water), positive: m/z 446.08 $[M + H]^+$.

Synthesis of copper(II) complexes

1·0.4H$_2$O·0.7C$_3$H$_7$OH. To a solution of **HL^1** (169 mg, 0.48 mmol) in isopropanol (8 mL) a solution of $CuCl_2{\cdot}2H_2O$ (82 mg, 0.48 mmol) in methanol (0.5 mL) was added. The reaction mixture was heated to reflux for 15 min, cooled down and allowed to stand at 4 °C overnight. The product was filtered off, washed with isopropanol and dried *in vacuo* to give a green-brown powder. Yield: 232 mg, 99%. Anal. Calcd for $C_{22}H_{17}Cl_2CuN_5{\cdot}0.4H_2O{\cdot}0.7C_3H_7OH$ (M 535.13 g mol^{-1}): C, 53.86; H, 4.24, N, 13.08. Found: C, 54.09; H, 4.41; N, 13.08. Solubility in water/1% DMSO ≥ 1.0 mg mL^{-1}. ESI-MS (acetonitrile/methanol + 1% water), positive: m/z 764.23 $[Cu^{II}(\mathbf{L^1})(\mathbf{HL^1})]^+$.

2·0.5H$_2$O. To a solution of **HL^2** (100 mg, 0.23 mmol) in isopropanol (20 mL) at 70 °C a solution of $CuCl_2{\cdot}2H_2O$ (40 mg, 0.23 mmol) in methanol (1 mL) was added. The colour of the solution changed from yellow to green and the reaction mixture was refluxed for 15 min. After cooling down the solution was kept at 4 °C overnight. Green precipitate was filtered off, washed with isopropanol and dried *in vacuo*. Yield: 105 mg, 77%. Anal. Calcd for $C_{22}H_{16}BrCl_2CuN_5{\cdot}0.5H_2O$ (M 573.76 g mol^{-1}): C, 46.05; H, 2.99, N, 12.21. Found: C, 45.93; H, 2.86; N, 12.52. Solubility in water/1% DMSO ≥ 0.7 mg mL^{-1}. ESI-MS (acetonitrile/methanol + 1% water), positive: m/z 922.07 $[Cu^{II}(\mathbf{L^2})(\mathbf{HL^2})]^+$.

3·0.3H$_2$O·0.6C$_3$H$_7$OH. To a solution of **HL^3** (200 mg, 0.55 mmol) in isopropanol (140 mL) at 70 °C a solution of $CuCl_2{\cdot}2H_2O$ (95 mg, 0.55 mmol) in methanol (1 mL) was added. The colour of the solution changed from yellow to green and the mixture was refluxed for 15 min. After cooling down the solution was kept at 4 °C overnight. The next day a green precipitate was filtered off, washed with isopropanol and dried *in vacuo*. Yield: 224 mg, 82%. Anal. Calcd for $C_{23}H_{19}Cl_2CuN_5{\cdot}0.3H_2O{\cdot}0.6C_3H_7OH$ (M 541.34 g mol^{-1}): C, 55.02; H, 4.54, N, 12.94. Found: C, 55.07; H, 4.16; N, 12.84. Solubility in water/1% DMSO ≥ 0.3 mg mL^{-1}. ESI-MS (acetonitrile/methanol + 1% water), positive: m/z 463.04 $[CuCl(\mathbf{HL^3})]^+$, 427.07 $[Cu(\mathbf{L^3})]^+$.

4·0.5H$_2$O. To a solution of **HL^4** (50 mg, 0.11 mmol) in isopropanol (20 mL) at 70 °C $CuCl_2{\cdot}2H_2O$ (19 mg, 0.11 mmol) in methanol (1 mL) was added. The colour of the solution changed from yellow to green and the reaction mixture was refluxed for 15 min. After cooling to room temperature, the solution was kept at 4 °C overnight. The next day a green precipitate was filtered off, washed with isopropanol and dried *in vacuo*. Yield: 51 mg, 80%. Anal. Calcd for $C_{23}H_{18}BrCl_2CuN_5{\cdot}0.5H_2O$ (M 587.79 g mol^{-1}): C, 47.00; H, 3.26, N, 11.91. Found: C, 46.85; H, 3.53; N, 11.81. Solubility in water/1% DMSO ≥ 0.9 mg mL^{-1}. ESI-MS (acetonitrile/methanol + 1% water), positive: m/z 542.96 $[Cu^{II}Cl(\mathbf{HL^4})]^+$, 507.00 $[Cu^{II}(\mathbf{L^4})]^+$.

Crystallographic structure determination. X-ray diffraction quality single crystals of **HL^4** were obtained by crystallisation from ethanol, **1^{trim}**·2DMF·1.25H$_2$O, **3**·1.2DMF·0.25H$_2$O, **3′**·DMF and **4**·2DMF by slow diffusion of diethyl ether into the DMF solution of the corresponding complex, while **2**·0.55MeOH by slow evaporation of the metanolic solution of the compound. The measurements were performed on Bruker X8 APEXII CCD (**2**·0.55MeOH, **3**·1.2DMF·0.25H$_2$O) and Bruker D8 Venture (**HL^4**, **1^{trim}** ·2DMF·1.25H$_2$O, **3′**·DMF, **4**·2DMF) diffractometers. Single crystals were positioned at 27, 27, 27, 35, 25 and 27 mm from the detector, and 672, 1632, 1000, 614, 479 and 1566 frames were measured, each for 8, 30, 10, 24, 3 and 6 s over 0.4, 0.5, 0.5, 0.7, 0.5 and 0.5° scan width for **HL^4**, **1^{trim}**·2DMF·1.25H$_2$O, **2**·0.55MeOH, **3**·1.2DMF·0.25H$_2$O, **3′**·DMF and **4**·2DMF, respectively. The data were processed using SAINT software.[28] Crystal data, data collection parameters, and structure refinement details are given in Tables 1 and 2. The structures were solved by direct methods and refined by full-matrix least-squares techniques. Non-H atoms were refined with anisotropic displacement parameters. H atoms were inserted in calculated positions and refined with a riding model. Co-crystallised solvent molecules (DMF, H_2O or CH_3OH) were found to be disordered in **1^{trim}**, **2** and **3**. The positional parameters of disordered atoms were refined by using PART, DFIX, SADI and EADP tools implemented in SHELX. The following computer programs and hardware were used: structure solution, *SHELXS-2014* and refinement, *SHELXL-2014*;[29] molecular diagrams, ORTEP;[30] computer, Intel CoreDuo. CCDC 1903184–1903189.†

Spectrophotometric solution equilibrium studies. An Agilent Carry 8454 diode array spectrophotometer was used to record the UV-vis spectra in the interval 200–800 nm. The path length was 2 cm. Spectrophotometric titrations were performed on samples containing the proligand **HL^3** or the complex **3** at 12.5 μM concentration by a KOH solution in the presence of 0.1 M KCl in DMSO : water 30 : 70 (w/w) mixture as solvent at 25.0 ± 0.1 °C in the pH range from 2 to 11. An Orion 710A pH-meter equipped with a Metrohm combined electrode (type 6.0234.100) and a Metrohm 665 Dosimat burette were used for the pH measurements and titrations. The electrode system was

Table 1 Crystal data and details of data collection for HL^4, 1^{trim}·2DMF·1.25H_2O, 2·0.55MeOH, 3·1.2DMF·0.25H_2O

Compound	HL^4	1^{trim}·2DMF·1.25H_2O	2·0.55MeOH	3·1.2DMF·0.25H_2O
Empirical formula	$C_{23}H_{18}BrN_5$	$C_{72}H_{67.5}Cl_6Cu_3N_{17}O_{3.25}$	$C_{22.55}H_{18.2}BrCl_2CuN_5O_{0.55}$	$C_{26.6}H_{27.9}Cl_2CuN_{6.2}O_{1.45}$
fw	444.33	1626.25	582.37	592.09
Space group	$P2_1/c$	$P\bar{1}$	$C2/c$	$P\bar{1}$
a [Å]	18.405(4)	13.0443(3)	37.232(30)	9.7602(13)
b [Å]	8.2958(16)	14.9957(3)	11.3330(11)	13.4027(15)
c [Å]	13.230(3)	20.2999(4)	11.6674(10)	20.685(2)
α [°]		92.0747(8)		98.235(4)
β [°]	103.962(8)	103.4914(8)	107.494(3)	92.013(5)
γ [°]		112.4054(8)		93.367(4)
V [Å^3]	1960.4(7)	3535.02(13)	4695.3(7)	2670.7(5)
Z	4	2	8	4
λ [Å]	0.71073	0.71073	0.71073	0.71073
ρ_{calcd} [g cm^{-3}]	1.506	1.528	1.648	1.473
Crystal size [mm]	0.10 × 0.08 × 0.01	0.14 × 0.08 × 0.06	0.13 × 0.10 × 0.02	0.80 × 0.08 × 0.08
T [K]	100(2)	100(2)	100(2)	296(2)
μ [mm^{-1}]	2.117	1.183	2.883	1.053
$R_1{}^a$	0.0527	0.0387	0.0599	0.0725
$wR_2{}^b$	0.1203	0.0984	0.1650	0.1719
GOF^c	1.041	1.033	1.149	0.943

$^a R_1 = \sum||F_o| - |F_c||/\sum|F_o|$. $^b wR_2 = \{\sum[w(F_o{}^2 - F_c{}^2)^2]/\sum[w(F_o{}^2)^2]\}^{1/2}$. ^{c} GOF = $\{\sum[w(F_o{}^2 - F_c{}^2)^2]/(n-p)\}^{1/2}$, where n is the number of reflections and p is the total number of parameters refined.

Table 2 Crystal data and details of data collection for 3′·DMF and 4·2DMF

Compound	3′·DMF	4·2DMF
Empirical formula	$C_{26}H_{25}ClCuN_6O$	$C_{29}H_{32}BrCl_2CuN_7O_2$
fw	536.51	724.97
Space group	$P2_1/c$	$P\bar{1}$
a [Å]	10.3347(4)	12.0530(9)
b [Å]	23.4454(7)	16.7234(14)
c [Å]	11.0757(4)	17.8152(15)
α [°]		105.698(3)
β [°]	117.731(1)	105.962(3)
γ [°]		106.665(3)
V [Å^3]	2375.41(15)	3060.2(4)
Z	4	4
λ [Å]	0.71073	0.71073
ρ_{calcd} [g cm^{-3}]	1.500	1.574
Crystal size [mm]	0.10 × 0.08 × 0.05	0.19 × 0.08 × 0.03
T [K]	100(2)	100(2)
μ [mm^{-1}]	1.065	2.234
$R_1{}^a$	0.0566	0.0498
$wR_2{}^b$	0.1597	0.1177
GOF^c	1.031	1.024

$^a R_1 = \sum||F_o| - |F_c||/\sum|F_o|$. $^b wR_2 = \{\sum[w(F_o{}^2 - F_c{}^2)^2]/\sum[w(F_o{}^2)^2]\}^{1/2}$. ^{c} GOF = $\{\sum[w(F_o{}^2 - F_c{}^2)^2]/(n-p)\}^{1/2}$, where n is the number of reflections and p is the total number of parameters refined.

calibrated to the pH = −log[H$^+$] scale in the DMSO–water solvent mixture by means of blank titrations (HCl *vs.* KOH) similarly to the method suggested by Irving *et al.* in pure aqueous solutions.[31] The average water ionisation constant (pK_w) was 14.52 ± 0.05, which corresponds well to the literature data.[32] Argon was passed over the solutions during the titrations. Proton dissociation constants (pK_a) of the ligand, overall stability constants (log β) of the copper(II) complexes and the individual spectra of the various species present in solution were calculated by the computer program PSEQUAD.[33] β ($M_pL_qH_r$) is defined for the general equilibrium $pM + qL + rH \rightleftharpoons M_pL_qH_r$ as β ($M_pL_qH_r$) = $[M_pL_qH_r]/[M]^p[L]^q[H]^r$ where M denotes the copper(II) ion and L the completely deprotonated ligand. The calculations were always performed from the experimental titration data measured in the absence of any precipitate in the solution.

Attempts to determine distribution coefficients ($D_{7.4}$) of HL^1, HL^3 and complexes **1**, **3** were undertaken by the traditional shake-flask method in *n*-octanol/buffered aqueous solution at pH 7.40 (20 mM phosphate buffer, 0.10 M KCl) as described previously.[34]

Cyclic voltammetry and spectroelectrochemistry. Cyclic voltammetric experiments with 0.5 mM solutions of **1–4** in 0.1 M nBu$_4$NPF$_6$ (puriss quality from Fluka; dried under reduced pressure at 70 °C for 24 h before use) supporting electrolyte in DMSO (SeccoSolv max. 0.025% H_2O, Merck) were performed under argon atmosphere using a three-electrode arrangement with platinum wire as counter electrode, and silver wire as pseudoreference electrode. Glassy carbon (GC) or platinum disc served as working electrodes. Ferrocene purchased from Sigma Aldrich was used as the internal potential standard without further purification. All potentials in voltammetric studies were quoted *vs.* ferricenium/ferrocene (Fc^+/Fc) redox couple. A Heka PG310USB (Lambrecht, Germany) potentiostat with a PotMaster 2.73 software package served for the potential control in voltammetric studies. *In situ* ultraviolet-visible-near-infrared (UV-vis-NIR) spectroelectrochemical measurements were performed on a spectrometer (Avantes, Model AvaSpec-2048x14-USB2 in the spectroelectrochemical cell kit (AKSTCKIT3) with the Pt-microstructured honeycomb working electrode, purchased from Pine Research Instrumentation. The cell was positioned in the CUV-UV Cuvette Holder (Ocean Optics) connected to the diode-array UV-vis-NIR spectrometer by optical fibers. UV-vis-NIR spectra were processed using the

AvaSoft 7.7 software package. Halogen and deuterium lamps were used as light sources (Avantes, Model AvaLight-DH-S-BAL).

Cell lines. Human colonic adenocarcinoma cell lines Colo 205 doxorubicin-sensitive (ATCC-CCL-222) and Colo 320/MDR-LRP multidrug resistant over-expressing ABCB1 (MDR1)-LRP (ATCC-CCL-220.1) were purchased from LGC Promochem, Teddington, UK. The cells were cultured in RPMI 1640 medium supplemented with 10% heat-inactivated fetal bovine serum, 2 mM L-glutamine, 1 mM Na-pyruvate and 10 mM HEPES. The cell lines were incubated at 37 °C, in a 5% CO_2, 95% air atmosphere. The semi-adherent human colon cancer cells were detached with Trypsin-Versene (EDTA) solution for 5 min at 37 °C. MRC-5 human embryonal lung fibroblast cell line (ATCC CCL-171) was purchased from LGC Promochem, Teddington, UK. The cells were cultured in Eagle's Minimal Essential Medium (EMEM, containing 4.5 g L^{-1} glucose) supplemented with a non-essential amino acid mixture, a selection of vitamins and 10% heat-inactivated fetal bovine serum. The cell lines were incubated at 37 °C, in a 5% CO_2, 95% air atmosphere.

Assay for cytotoxic effect. MRC-5 non-cancerous human embryonic lung fibroblast and human colonic adenocarcinoma cell lines (doxorubicin-sensitive Colo 205 and multidrug resistant Colo 320 colonic adenocarcinoma cells) were used to determine the effect of compounds on cell growth. The effects of increasing concentrations of compounds on cell growth were tested in 96-well flat-bottomed microtiter plates. The compounds were dissolved in DMSO and stock solutions of 10 mM were prepared. These were further diluted in the appropriate cell culture medium by 2-fold serial dilution starting from 100 μM to 0.195 μM. The adherent human embryonal lung fibroblast cells were cultured in 96-well flat-bottomed microtiter plates, using EMEM supplemented with 10% heat-inactivated fetal bovine serum. The density of the cells was adjusted to 1×10^4 cells in 100 μL per well, the cells were seeded for 24 h at 37 °C, 5% CO_2, then the medium was removed from the plates containing the cells, and the dilutions of compounds previously made in a separate plate were added to the cells in 200 μL. In case of the colonic adenocarcinoma cells, the two-fold serial dilutions of compounds were prepared in 100 μL of RPMI 1640, horizontally. The semi-adherent colonic adenocarcinoma cells were treated with Trypsin-Versene (EDTA) solution. They were adjusted to a density of 1×10^4 cells in 100 μL of RPMI 1640 medium, and were added to each well, with the exception of the medium control wells. The final volume of the wells containing compounds and cells was 200 μL. The culture plates were incubated at 37 °C for 72 h; at the end of the incubation period, 20 μL of MTT (thiazolyl blue tetrazolium bromide, Sigma) solution (from a stock solution of 5 mg mL^{-1}) were added to each well. After incubation at 37 °C for 4 h, 100 μL of sodium dodecyl sulfate (SDS) (Sigma) solution (10% in 0.01 M HCl) were added to each well and the plates were further incubated at 37 °C overnight. Cell growth was determined by measuring the optical density (OD) at 540/630 nm with Multiscan EX ELISA reader (Thermo Labsystems, Cheshire, WA, USA). Inhibition of the cell growth was determined according to the formula below:

$$IC_{50} = 100 - \left[\frac{\text{OD sample} - \text{OD medium control}}{\text{OD cell control} - \text{OD medium control}}\right] \times 100$$

Results are expressed in terms of IC_{50}, defined as the inhibitory dose that reduces the growth of the cells exposed to the tested compounds by 50%. The IC_{50} values were calculated using GraphPad Prism7 software.

Results and discussion

Synthesis

The synthesis of the main core structure **A** in Chart 2 was performed by following the published literature protocols. **B** was synthesised similarly.[18–20] A detailed description for the synthesis of **B** is given in the ESI.† The lactam derivatives **A** and **B** were converted into thiolactams **C** and **D** by reaction with P_2S_5 on Al_2O_3 in dry boiling acetonitrile or tetrahydrofuran in 82 and 60% yield, respectively.[27] Thionation with phosphorus pentasulfide bound to aluminium oxide offers the advantage that the reagent can be removed by filtration after the reaction. In addition, this method was chosen because the standard method for the thionation of paullones[10] gave only small yields. Further reaction of **C** and **D** with hydrazine hydrate as reagent and solvent afforded hydrazines **E** and **F** in 86 and 92% yield, respectively. It should be noted that **F** exists in two tautomeric forms in DMSO solution, as evidenced by the appearance of two signal sets in the ^{1}H NMR spectrum. The predominant species is the one shown in Chart 2 where N^{13} is protonated and the double bond is endocyclic. The NMR signal of $N^{13}H$ appears as a singlet at δ = 6.36 ppm. In the minor species, (*ca.* 15% in DMSO), N^6 is protonated and the double bond is exocyclic. N^6H appears as a triplet with the typical coupling constant of 5.3 Hz at δ = 8.49 ppm. NMR data is given only for the major species in the experimental part, because of the low signal intensity of the minor species and signal overlapping. For atom numbering scheme see Scheme S1, ESI.† Similar tautomerism has been observed in the case of paullones previously.[14] The Schiff bases $\mathbf{HL^1}$–$\mathbf{HL^4}$ were prepared in 99, 31, 94 and 58% yield, respectively, from hydrazine species **E** and **F** and 2-formyl- and 2-acetylpyridine taken in 10% excess in boiling ethanol. ^{1}H and ^{13}C NMR spectra of $\mathbf{HL^1}$–$\mathbf{HL^4}$ were in agreement with the formulae proposed. Notably, $\mathbf{HL^4}$ showed a second set of NMR-signals with an intensity of about 10% of the main species in DMSO-d_6. Tautomerism as in the case for **F** was excluded, because of the presence of the typical triplet signal for N^6H in both species. It is likely that a mixture of *E* and *Z* isomers is present, similarly to previously reported paullone derived ruthenium(II) and osmium(II) complexes.[17] However, low signal intensity and signal overlapping did not allow a more accurate analysis to be performed. ESI mass spectra measured in positive ion mode showed peaks with *m*/*z* 352.26, 432.06, 366.16 and 446.08 attributed to $[M + H]^+$. The purity of $\mathbf{HL^1}$–$\mathbf{HL^4}$ (>95%) was con-

firmed by elemental analysis. The structure of $\mathbf{HL^4}$ was also established by single crystal X-ray diffraction (*vide infra*). Complexes **1–4** were prepared by reaction of $\mathbf{HL^1}$–$\mathbf{HL^4}$ in isopropanol by addition of a methanolic solution of $CuCl_2{\cdot}2H_2O$ in 1 : 1 mol ratio, respectively, in 77 to 99% yields. The positive ion ESI mass spectrum of **1** showed the presence of a peak with *m*/*z* 764.18 due to $[Cu^{II}(\mathbf{L^1})(\mathbf{HL^1})]^+$. The mass spectra of **2–4** contain peaks at *m*/*z* 528.97 and 492.99, 463.04 and 427.07, 542.96 and 507.00 attributed to $[Cu^{II}Cl(\mathbf{HL^{2-4}})]^+$ and $[Cu^{II}(\mathbf{L^{2-4}})]^+$, respectively. The elemental analysis was in agreement with the structures shown in Chart 2, providing the required purity of bulk samples for biological investigations. The complexes **1–4** as well as **3′** have been studied by X-ray diffraction.

X-ray diffraction

The results of X-ray diffraction studies for $\mathbf{1^{trim}}$, **2**, **3**, **3′**, **4** and $\mathbf{HL^4}$ are shown in Fig. 1–3, respectively, with selected bond lengths and bond angles quoted in the legends. Complex **1** crystallised as a trimer ($\mathbf{1^{trim}}$), while **2–4** and **3′** as monomeric entities. The corresponding ligand is protonated in $\mathbf{1^{trim}}$, **2–4** and acts as a tridentate one being coordinated to copper(II) *via* azepine nitrogen, hydrazine nitrogen and pyridine nitrogen atoms. The ligands can be deprotonated in the presence of a base. In particular, deprotonation of $\mathbf{HL^3}$ in **3** in the presence of triethylamine was confirmed by X-ray diffraction study of **3′** (Fig. 2b). The coordination geometry of copper(II) ion in the trimer ($\mathbf{1^{trim}}$) and in mononuclear complexes **2–4** is square-pyr-

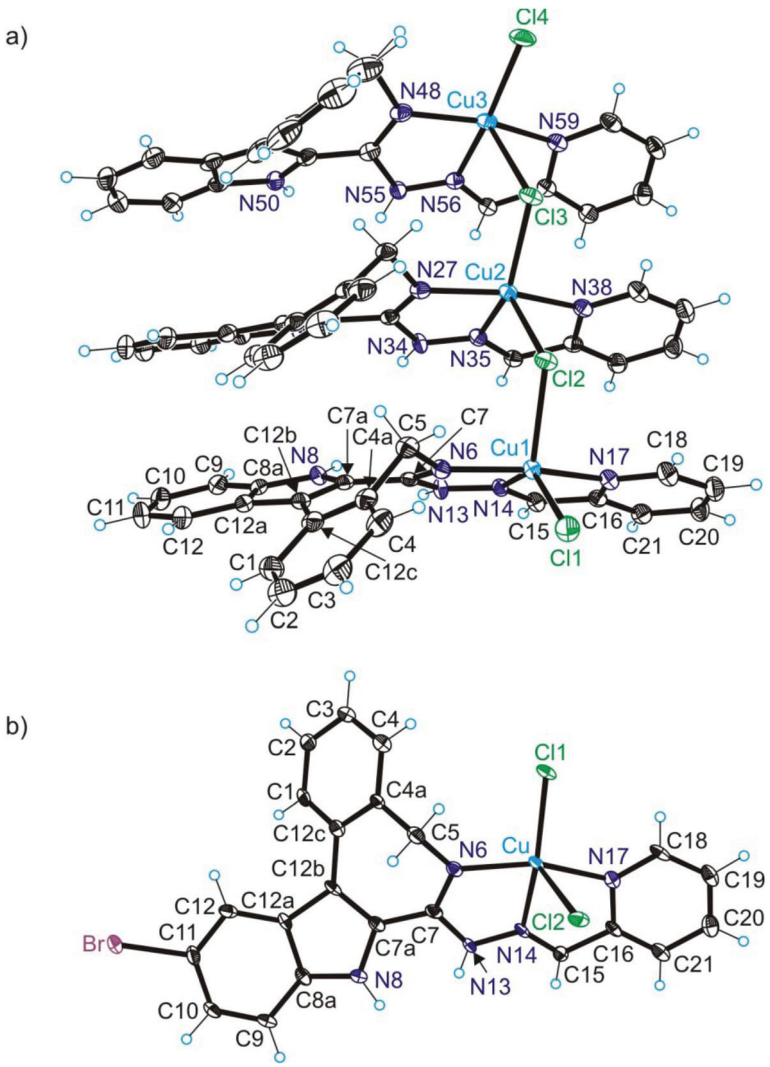

Fig. 1 ORTEP views of (a) the complex cation $[Cu_3Cl_4(\mathbf{HL^1})_3]^{2+}$ in $\mathbf{1^{trim}}$ and (b) of $[CuCl_2(\mathbf{HL^2})]$ in **2**. Selected bond distances (Å) and bond angles (deg) in $\mathbf{1^{trim}}$: Cu1–N6 1.994(2), Cu1–N14 1.991(2), Cu1–N17 2.044(2), Cu1–Cl1 2.2685(8), Cu1–Cl2 2.4382(7), N6–Cu1–N14 78.75(10), N14–Cu1–N17 77.92(9), Cu2–N27 1.990(2), Cu2–N35 1.975(2), Cu2–N38 2.034(2), Cu2–Cl2 2.4492(8), Cu2–Cl3 2.2781(8), N27–Cu2–N35 79.39(10), N35–Cu2–N38 78.63(10), Cu3–N48 1.995(3), Cu3–N56 1.959(2), Cu3–N59 2.044(2), Cu3–Cl3 2.6404(8), Cu3–Cl4 2.2116(8), N48–Cu3–N56 79.51(10), N56–Cu3–N59 79.20(10). Details of coordination geometry in $\mathbf{1^{trim}}$: τ_5 (Cu1) = 0.35, τ_5 (Cu2) = 0.25, τ_5 (Cu3) = 0.17; in **2**: Cu–N6 1.982(5), Cu–N14 1.971(5), Cu–N17 2.051(5), Cu–Cl1 2.2252(16), Cu–Cl2 2.5762(17), N6–Cu–N14 79.7(2), N14–Cu–N17 78.8(2). Details of coordination geometry in **2**: τ_5 (Cu) = 0.06.

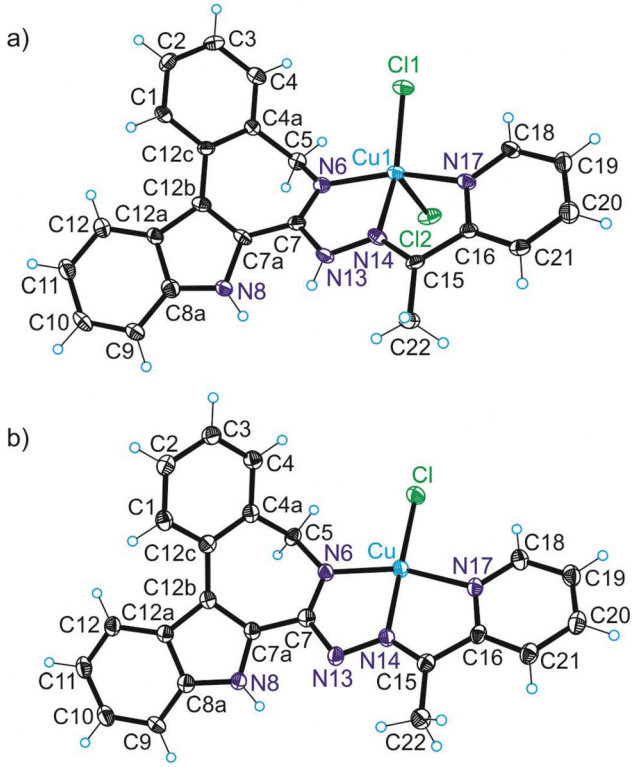

Fig. 2 ORTEP views of (a) one crystallographically independent complex $[CuCl_2(HL^3)]$ in **3** (co-crystallised solvent is omitted) and (b) of $[CuCl(L^3)]$ in **3′**. Selected bond distances (Å) and bond angles (deg) in **3**: Cu1–N6 1.979(4), Cu1–N14 1.973(4), Cu1–N17 2.034(4), Cu1–Cl1 2.2460(12), Cu1–Cl2 2.4566(14), N6–Cu1–N14 78.72(17), N14–Cu1–N17 78.33(16), Cu2–N28 1.986(5), Cu2–N36 1.969(4), Cu2–N39 2.031(4), Cu2–Cl3 2.2309(14), Cu2–Cl4 2.5054(13), N28–Cu2–N36 79.09(17), N36–Cu2–N39 78.36(18). Details of coordination geometry in **2**: τ_5 (Cu1) = 0, τ_5 (Cu2) = 0.06 (second crystallographically independent molecule); in **3′**: Cu–N6 1.937(3), Cu–N14 1.953(3), Cu–N17 2.019(3), Cu–Cl 2.2058(9), N6–Cu–N14 79.52(12), N14–Cu–N17 80.27(12).

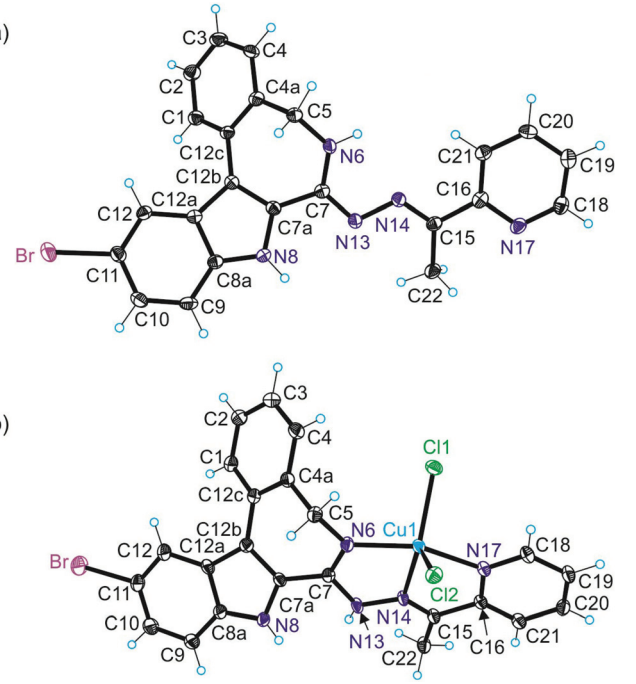

Fig. 3 ORTEP views of (a) proligand HL^4 and (b) of $[CuCl_2(HL^4)]$ in **4** (co-crystallised solvent is omitted). Selected bond distances (Å) and bond angles (deg) in HL^4: C5–N6 1.459(4), N6–C7 1.344(4), C7–N13 1.325(4), N13–N14 1.391(3), N14–C15 1.300(4); in **4**: Cu1–N6 2.011(2), Cu1–N14 1.986(2), Cu1–N17 2.057(3), Cu1–Cl1 2.2612(8), Cu1–Cl2 2.4327(9), C5–N6 1.470(4), N6–C7 1.295(4), C7–N13 1.376(4), N13–N14 1.366(3), N14–C15 1.285(4), N6–Cu1–N14 78.83(10), N14–Cu1–N17 77.34(10), Cu2–N28 2.010(2), Cu2–N36 1.968(2), Cu2–N39 2.035(3), Cu2–Cl3 2.2204(8), Cu2–Cl4 2.5321(9), N28–Cu2–N36 79.40(10), N36–Cu2–N39 78.40(10). Details of coordination geometry in **4**: τ_5 (Cu1) = 0.28, τ_5 (Cu2) = 0.28 (second crystallographically independent molecule).

amidal or distorted square-pyramidal (see legends to Fig. 1–3 quoting τ_5-descriptor values[35] for each copper(II) ion), while in **3′** it is slightly distorted square-planar. The coordination polyhedron in each case is completed by two or one chlorido co-ligands. Note that the same coordination geometry was previously established for complexes **5** and **6** with paullone derivatives (τ_5 = 0.10 (**5**) and 0.05 (**6**)).[15] The bond lengths Cu–N5 = 2.038(3) and 2.0220(15), Cu–N14 = 1.982(3) and 1.9787(15), Cu–N17 = 2.062(3) and 2.0466(15) in **5** and **6**, respectively, are significantly longer than those in **2** and **3** (see legends to Fig. 1 and 2) by 0.01–0.05 and 0.005–0.04 Å, respectively, even though the metal binding moieties in the corresponding ligands are closely related. Overall a tighter binding of the ligand moiety in **2** and **3** is to be mentioned when compared to that in **5** and **6**. The proligand HL^4 and the ligand HL^4 in **4** adopt different configurations and distinct proton tautomeric forms as shown in Fig. 3 and confirmed by the distribution of bond lengths (electron density) over the fragment C5–N6–C7–N13–N14–C15 quoted in the legend to Fig. 3.

Of note is also that the two Cu–Cl bonds in **1–4** are markedly different. The bond length from copper(II) to basal chlorido co-ligand is by 0.17 to 0.43 Å shorter compared to that between copper(II) and the apical chlorido co-ligand. A similar situation is also typical for **5** and **6** reported previously.[15,25] The corresponding bonds differ by 0.19 and 0.13 Å in **5** and **6**, respectively.

Solution equilibrium studies

The proligand HL^3 and complex **3** (Charts 1 and 2) were chosen for the detailed solution equilibrium studies. Two complexes with HL^3 were obtained in the solid state, namely $[CuCl_2(HL^3)]$ (**3**) and $[CuCl(L^3)]$ (**3′**) (Fig. 2), in which the ligand adopts different protonation states. We therefore aimed to study the transformation process of **3** into **3′** in solution. Both HL^3 and complex **3** have fairly poor water solubility, thus UV-vis spectrophotometric titrations were performed in the presence of 30% (w/w) DMSO at low concentration (12.5 μM). The UV-vis spectra recorded for the proligand revealed small but characteristic changes upon increasing the pH (Fig. 4a) and two well separated proton dissociation processes could be observed. The first deprotonation process was accompanied by

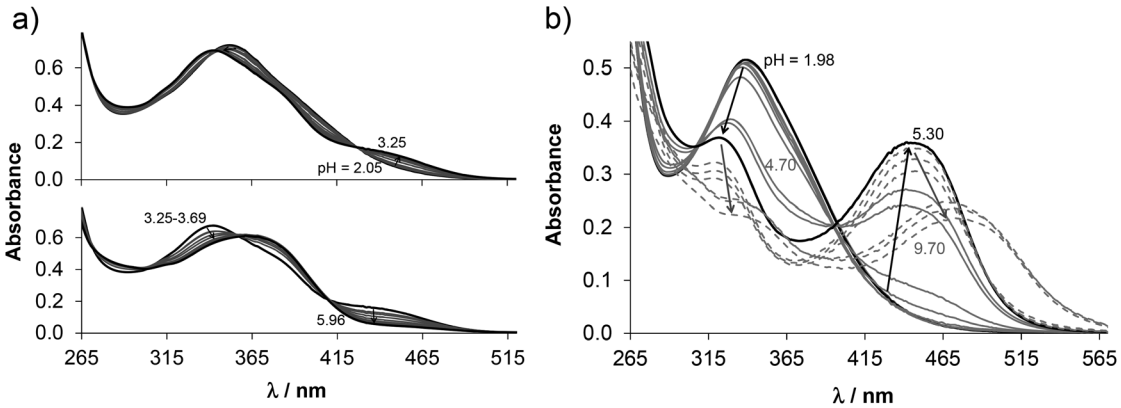

Fig. 4 UV-vis spectra recorded for (a) HL^3 and (b) complex **3** at various pH values in 30–70% (w/w) DMSO–water solvent mixture. {$c_{ligand} = c_{complex}$ = 12.5 μM; T = 298 K; I = 0.10 M (KCl); l = 2 cm}.

a blue shift (λ_{max}: 351 nm → 340 nm) and an absorbance increase at ~440 nm in the pH range between 2.5 and 3.25. The solution was yellow in this pH range. Upon increasing the pH the solution became colourless due to the decrease of absorbance in the visible wavelength range (415–490 nm) and the λ_{max} is red shifted (340 nm → 360 nm). At pH >6.5 precipitation occurred in the solution most likely due to the formation of the neutral species, thus data collected below this pH were used for the calculations. The pK_a values (Table 3) and the spectra of the individual ligand species (Fig. 5a) were calculated on the basis of deconvolution of recorded UV-vis spectra. The proligand $\mathbf{HL^3}$, which can be drawn in two tautomeric forms due to the rearrangement of the N=C–NH–N and NH–C=N–N bonds, contains two additional protons in its fully protonated form $(H_2(\mathbf{HL^3})^{2+}$, (Chart 4). The first deprotonation process (pK_{a1}) can presumably be attributed to deprotonation of the pyridinium nitrogen, while the second step (pK_{a2}) to the deprotonation of the benzazepinium nitrogen. The pK_a values were predicted by using the software MarvinSketch as well[36] (Table 3), showing the same order of the stepwise deprotonation processes as we suggest herein. However, these are somewhat different compared to the values obtained experimentally in the DMSO–water solvent mixture.

Table 3 Proton dissociation constants (K_a) of HL^3 and overall stability constants (β) of its copper(II) complexes determined by UV-vis titrations in 30–70% (w/w) DMSO–water solvent mixture, {T = 298 K; I = 0.10 M (KCl)}. Predicted pK_a and log $D_{7.4}$ values for HL^3 and HL^1 by the software MarvinSketch.[36]

	Constant		Predicted constant
pK_{a1} $H_2(\mathbf{HL^3})^{2+}$	2.51 ± 0.01	pK_{a1} $H_2(\mathbf{HL^3})^{2+}$	1.82
pK_{a2} $H(\mathbf{HL^3})^{+}$	5.03 ± 0.01	pK_{a2} $H(\mathbf{HL^3})^{+}$	5.37
log β $[Cu(\mathbf{HL^3})]^{2+}$	10.96 ± 0.02	log $D_{7.4}$ $\mathbf{HL^3}$	+4.03
log β $[Cu(\mathbf{L^3})]^{+}$	6.39 ± 0.02	pK_{a1} $H_2(\mathbf{HL^1})^{2+}$	2.00
log β $[Cu(\mathbf{L^3})(OH)]$	~−1.9	pK_{a2} $H(\mathbf{HL^1})^{+}$	5.39
pK_a $[Cu(\mathbf{HL^3})]^{2+}$	4.57	log $D_{7.4}$ $\mathbf{HL^1}$	+4.75
pK_a $[Cu(\mathbf{L^3})]^{+}$	~8.3		

The UV-vis spectrum recorded for **3** at pH ~2 (Fig. 4b) showed significant complex formation comparing to that of the free proligand. Thus the complex dissociates only partly under these conditions. Therefore, the tridentate coordination *via* the (*N*, *N*, *N*) donor set is assumed in $[Cu(\mathbf{HL^3})]^{2+}$ at such low pH. Upon increasing the pH the λ_{max} is shifted to the

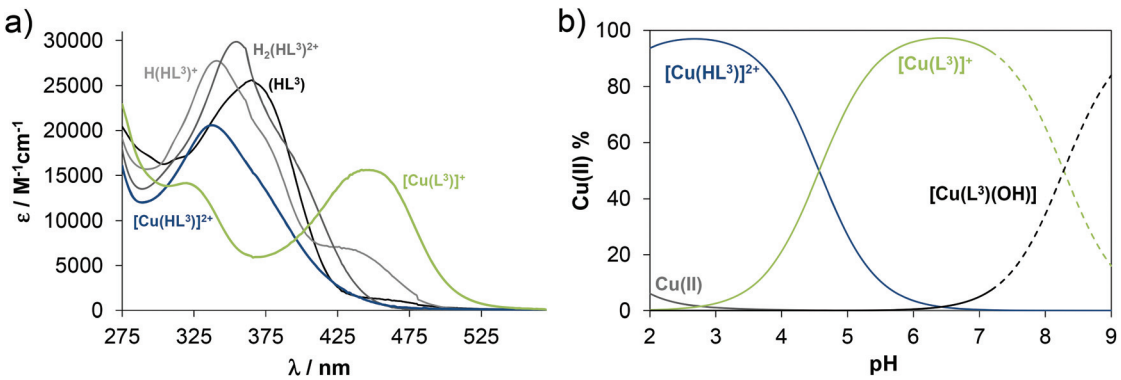

Fig. 5 (a) Molar absorbance spectra computed for proligand HL^3 and complex **3** in the various protonation states, and concentration distribution curves for **3** plotted against the pH. (Dashed lines show the region where precipitate appears.) {$c_{complex}$ = 12.5 μM; T = 298 K; I = 0.10 M (KCl); 30% (w/w) DMSO-H_2O}.

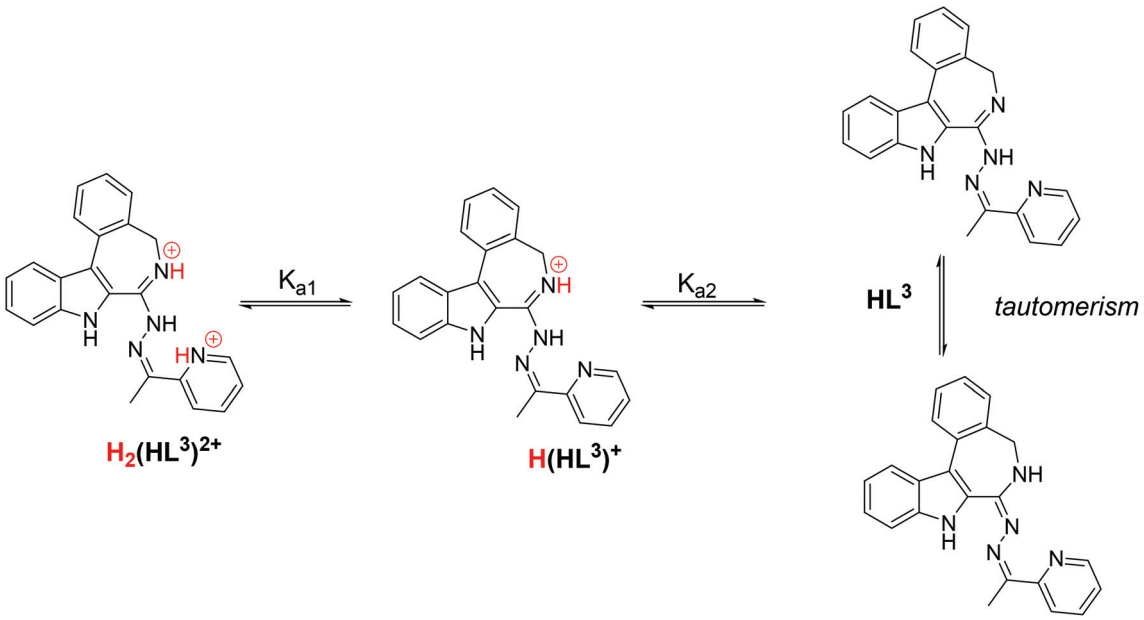

Chart 4 Stepwise deprotonation processes of the fully protonated form of HL^3 and its tautomeric forms.

lower wavelength (338 nm → 323 nm) concomitant with the development of a new band with λ_{max} 444 nm implying a rearrangement in the copper(II) chromophore. Most probably the non-coordinating hydrazinic nitrogen is deprotonated, as is the case with **3′** (Fig. 2b). In addition a novel process starts at pH >7 as the λ_{max} shows a further bathochromic shift (λ_{max} ~483 nm). Although it is accompanied by remarkable absorbance decrease in the whole wavelength range monitored due to the formation of precipitate of a neutral mixed hydroxido species [Cu($\mathbf{L^3}$)(OH)]. On the basis of the recorded UV-vis spectra overall stability constants for the complexes $[Cu(\mathbf{HL^3})]^{2+}$ and $[Cu(\mathbf{L^3})]^{+}$ were computed (Table 3) in addition to their individual spectra (Fig. 5a), while $\log\beta$ for [Cu($\mathbf{L^3}$)(OH)] could be only estimated. Concentration distribution curves were computed using the determined stability constants (Fig. 5b) revealing the predominant formation of $[Cu(\mathbf{L^3})]^{+}$ at neutral pH.

The lipo-hydrophilic character is an important property of drugs as it strongly affects the passage *via* biological membranes. Therefore we attempted to determine the $\log D_{7.4}$ values for proligands $\mathbf{HL^1}$, $\mathbf{HL^3}$ and complexes **1**, **3** using the traditional shake-flask method in *n*-octanol/buffered aqueous solution at pH 7.40. All these compounds were found to be so lipophilic that data could not be obtained experimentally since they remained in the octanol phase and only a minor fraction was found in the aqueous phase. Thus $\log D_{7.4}$ values were estimated for proligands $\mathbf{HL^1}$, $\mathbf{HL^3}$ by using the software MarvinSketch as well[36] (Table 3). The predicted values indicate the strong lipophilic character of the compounds. The bromo substituents in $\mathbf{HL^2}$, $\mathbf{HL^4}$ are suggested to increase the lipophilicity even more.

Electrochemistry and spectroelectrochemistry

Cyclic voltammograms of **1–4** in DMSO/nBu$_4$NPF$_6$ at glassy carbon (GC) working electrode show two irreversible reduction peaks with cathodic peak potentials at E^1_{pc} = −0.75 V and E^2_{pc} = −1.13 V for **1**, E^1_{pc} = −0.68 V and E^2_{pc} = −1.05 V for **2**, E^1_{pc} = −0.74 V and E^2_{pc} = −1.12 V for **3** and E^1_{pc} = −0.76 V and E^2_{pc} = −1.11 V for **4** *vs.* Fc^+/Fc (see Fig. 6 and Fig. S1, ESI†). The first irreversible reduction step can be attributed to the Cu(II) → Cu(I) process. We suppose that unstable [Cu(I)**L**] complex decomposes with partial or full release of the proligand. The follow-up product is then irreversibly reduced in the next reduction step.

To check the chemical reversibility of the first reduction step for **1–4**, the *in situ* spectroelectrochemical UV-vis-NIR experiments were carried out under an argon atmosphere in a special thin layer spectroelectrochemical cell with a microstructured honeycomb working electrode. The UV-vis spectra measured upon cathodic reduction of **1** revealed in the region of the first reduction peak a new emerging optical band at 385 nm. In addition, a decrease of the intensity of the bands at 275 and 485 nm is observed (Fig. 7a). According to the findings of the UV-vis titrations (Fig. 5a), these spectral changes suggest the dissociation of the Cu(II) complex and the liberation of the proligand.

Very similar spectroelectrochemical response was observed also for **2–4** in the region of the first reduction peak as illustrated for **3** in Fig. S2, ESI.† However, upon scan reversal the product that is formed upon reduction (Cu(II) to Cu(I)) is not reoxidised back to the initial state (Fig. 7b). This fact provides strong evidence that the Cu(I) oxidation state is unstable, resulting in the partial or complete decomposition of the complex. The presence of the Cu(II) ion in the cells may lead to the production of ROS *in vivo* because of Cu(II)/Cu(I) redox cycling due to Fenton like reactions.[37,38]

Cytotoxic activity assays

The latonduine derivatives $\mathbf{HL^1}$–$\mathbf{HL^4}$, their copper(II) complexes **1–4**, and the paullone derived copper(II) complexes **5**, **6** exhibi-

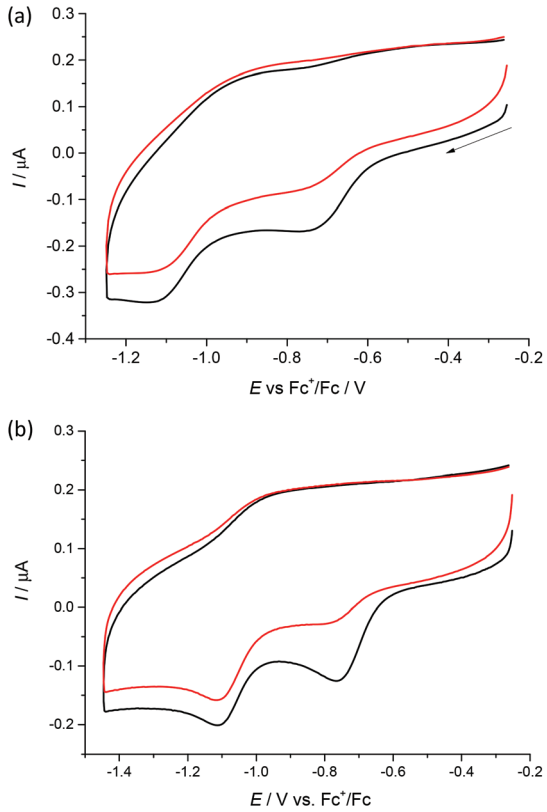

Fig. 6 Cyclic voltammograms of (a) **1** and (b) **4** in DMSO/nBu$_4$NPF$_6$ at scan rate of 100 mV s^{-1} at GC working electrode (black traces represent the first scan, while red traces the second scan).

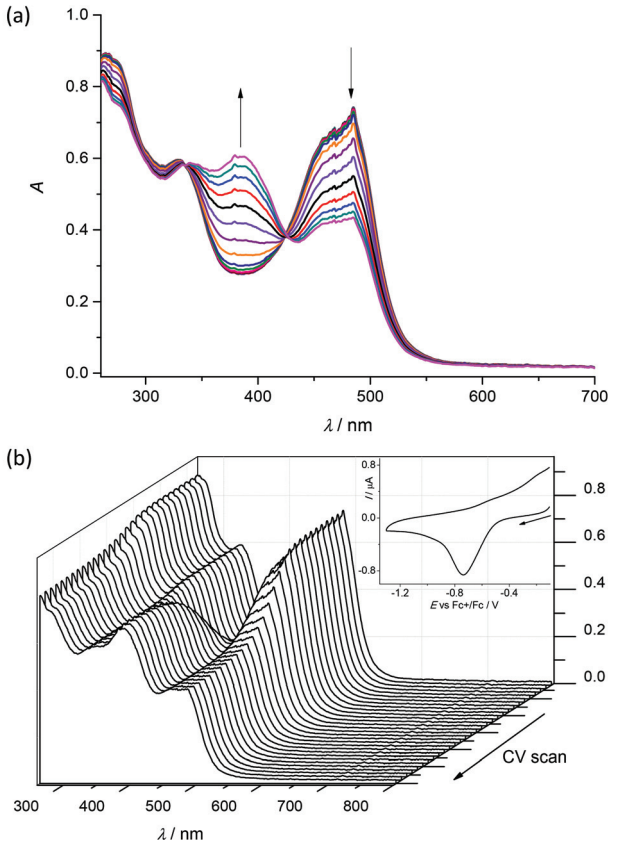

Fig. 7 *In situ* UV-vis-NIR spectroelectrochemistry for **1** in DMSO/nBu$_4$NPF$_6$ (scan rate of 10 mV s^{-1}, Pt-microstructured honeycomb working electrode): (a) evolution of UV-vis spectra in 2D projection in forward scan in the region of the first reduction peak; (b) UV-vis spectra detected simultaneously upon the cyclic voltammetric scan in 3D projection (Inset: The corresponding cyclic voltammogram).

ted strong cytotoxic activity in cancer cells, exceeding tremendously that of cisplatin. The latonduine derivatives **HL^1**–**HL^4** revealed strong cytotoxic activity in cancer cells, while they were less toxic in non-cancerous MRC-5 fibroblasts showing selectivity towards cancer cells (Table 4).

Interesting structure-activity and selectivity relationships deserve to be mentioned. Acetylpyridine derived proligands **HL^3** and **HL^4** were by one order of magnitude more cytotoxic than formylpyridine derived **HL^1** and **HL^2**. Bromo substituted **HL^2** and **HL^4** were about twice as cytotoxic compared to their unsubstituted counterparts **HL^1** and **HL^3**. The bromo substituted proligands **HL^2** and **HL^4** were not only more active, but they also showed a more pronounced selectivity for cancer cells over normal cells, by a factor of 2 to 25 compared to unsubstituted analogues **HL^1** and **HL^3** (see Table 4). Interestingly **HL^2** is more active in the multidrug resistant Colo 320 cell line than in the chemosensitive Colo 205 cell line with selectivity factors of 45 *vs.* 12, respectively. The most active proligand, **HL^4**, shows IC$_{50}$ values in the nanomolar range and is around 70 times more toxic in the cancer cell lines (Colo 205, Colo 320) than in the normal fibroblast MRC-5 cell line.

Formylpyridine derived copper(II) complexes **1** and **2** showed activity comparable to the respective proligands **HL^1** and **HL^2**, however, their selectivity for cancer cells over non-cancerous cell line is diminished. Copper(II) complex **2** was more active in the chemoresistant Colo 320 cancer cell line than in the chemosensitive Colo 205 cell line, similar to **HL^2**, leading to the assumption that proligand **HL^2** and copper(II) complex **2** may interfere with the ABCB1 transporter (P-glycoprotein). This is the first characterised ATP-binding cassette (ABC) transporter, which is the most studied member of this protein superfamily. ABC transporters bind and hydrolyse ATP to provide energy needed to transport/extrude the substrates/drugs *via* the cell membranes. It has been shown that the overexpression of this protein is often associated with the development of multidrug resistant phenotype in cancer and disadvantageous clinical prognosis.[39] An emerging research approach is the use of efflux pump inhibitors as adjuvant compounds (so-called "chemosensitisers") to improve the efficacy of antitumour therapy, by co-administering them with chemotherapeutic agents. Computer-aided drug design techniques are used for the rapid assessment of chemical libraries in order to guide and speed up the early-stage development of new active compounds. In order to determine the ability of the compounds investigated in the present study to interact with P-glycoprotein molecular docking calculations based on crys-

Table 4 The IC_{50} values for latonduine derivatives HL^1–HL^4 and their copper(II) complexes **1–4**, as well as for copper(II) complexes with paullones **5**, **6**. *Selectivity factors (SFs) for Colo 205 and Colo 320 cancer cell lines over non-cancerous MRC-5 cells. $SF_{(205)}$ = IC_{50} MRC-5/IC_{50} Colo 205, $SF_{(320)}$ = IC_{50} MRC-5/IC_{50} Colo 320

	IC_{50} (μM), 72 h				
	Colo 205	Colo 320	MRC-5	$SF_{(205)}$*	$SF_{(320)}$*
HL^1	0.266 ± 0.012	0.294 ± 0.005	1.522 ± 0.547	6	5
HL^2	0.189 ± 0.040	0.051 ± 0.012	2.312 ± 0.032	12	45
HL^3	0.037 ± 0.004	0.042 ± 0.001	0.127 ± 0.004	3	3
HL^4	0.017 ± 0.002	0.018 ± 0.005	1.257 ± 0.463	74	70
1	0.346 ± 0.008	0.315 ± 0.023	0.461 ± 0.069	—	—
2	0.556 ± 0.028	0.104 ± 0.002	0.378 ± 0.004	—	4
3	0.017 ± 0.001	0.020 ± 0.001	0.162 ± 0.009	10	8
4	0.007 ± 0.001	0.015 ± 0.002	0.201 ± 0.001	29	13
5	1.704 ± 0.218	0.413 ± 0.044	0.152 ± 0.001	—	—
6	0.380 ± 0.032	0.120 ± 0.007	0.061 ± 0.003	—	—
Cisplatin	31.94 ± 2.17	4.81 ± 0.68	12.41 ± 0.367	—	3

tallographic data reported by Ferreira *et al.*[40] will be performed and the results will be reported in due course.

Acetylpyridine derived complexes **3** and **4** are by one to two orders of magnitude more active than their formylpyridine derived analogues **1** and **2** and about twice as cytotoxic as the corresponding proligands HL^3 and HL^4. The strong enhancement of cytotoxicity, when a methyl group is present at the imine carbon of the ligand, has been observed also in the case of paullone derived copper(II) complexes previously.[15,25] Compound **4** is the most active drug in the whole series, with an astonishingly low IC_{50} value of 7 nM in the Colo 205 cancer cell line, being superior to the corresponding proligand HL^4 with IC_{50} value of 17 nM in the same cell line. The presence of bromo-substituent in position 9 of the paullone[41] or similar position in latonduine derivative and ketimine group instead of aldimine one increases the cytotoxic activity of both proligands and metal complexes, but we do not have any explanation of this observation at the molecular level now. Even though **4** is more cytotoxic to MRC-5 cells than HL^4, it still shows marked selectivity for cancer cells over normal ones, with selectivity factors of 29 and 13 for the Colo 205 and Colo 320 cancer cell lines, respectively. Paullone derived complexes **5** and **6** are isomers of latonduine derived complexes **2** and **3**. Intriguingly, **5** and **6** are less cytotoxic in the cancer cell lines (Colo 205, Colo 320) and more cytotoxic in MRC-5 cells, when compared to their counterparts **2** and **3**. This means that the new latonduine derived copper(II) complexes presented in this work offer both enhanced activity and selectivity in comparison with previously reported paullone derivatives.

Conclusions

Four new proligands, which can be regarded as biologically active latonduine modified or isomeric to paullone derivatives and containing a potentially tridentate metal binding site, HL^1–HL^4 were prepared *via* a multistep synthesis. In addition, four copper(II) complexes **1–4** were synthesised by direct complex formation reactions of proligands with $CuCl_2{\cdot}2H_2O$. For comparison two copper(II) complexes with paullone modified ligands reported previously, namely **5** and **6**, were also used in this study. These two complexes form isomeric pairs with **2** and **3**, respectively. The following features can be outlined from the performed investigations of the listed compounds. X-ray diffraction studies revealed, that like **5** and **6**, complexes **1–4** are five-coordinate and adopt a square-pyramidal or slightly distorted square-pyramidal coordination geometry. Deprotonation of the ligand HL^3 in **3** resulted in formation of **3′**, in which a square-planar coordination geometry is adopted by copper(II) as confirmed by single crystal X-ray crystallography. The decrease of coordination number of copper(II) from five in **3** to four in **3′** led to shortening of Cu–N and Cu–Cl bond lengths due to less repulsion between the ligand/donor atoms (see legend to Fig. 2 for comparison of bond lengths in the two complexes). It should be also noted that the ligands HL^2 and HL^3 are bound stronger in terms of bond lengths to copper(II) when compared to those in isomeric paulone-based complexes **5** and **6**, respectively. The Cu–N bond lengths were found to be by 0.01–0.05 and 0.005–0.04 Å shorter in **2** and **3** than in **5** and **6**, respectively. All the studied compounds are significantly lipophilic, and the proligands are in their neutral forms (**HL**) in solution at neutral pH (in 30% DMSO/H_2O), while complexes are found in their $[Cu(\mathbf{L})]^+$ forms under these conditions.

Cell tests showed that the new proligands and copper(II) complexes are highly active against Colo 205 and Colo 320 cancer lines and show selectivity for cancer cell lines over MRC-5, a non-cancerous fibroblast cell line. Structure-activity relationships were established, revealing that a methyl substituent at the imine carbon leads to a distinct enhancement of the cytotoxicity of the new proligands and copper(II) complexes and that a bromo substituent at position 11 of the indolo[2,3-*d*]benzazepine backbone enhances the activity as well as the selectivity. Intriguingly, complexes **2** and **3** were by factors 3 and 22 and by factors 4 and 6 more cytotoxic against Colo 205 and Colo 320 cells in terms of IC_{50} values than paullone-based complexes **5** and **6**. In contrast, in non-cancerous cells **5** and **6** were more cytotoxic by factors 2.5 and 2.6 than **2** and **3**,

respectively. So, the new complexes **2** and **3** appear to be superior to isomeric copper(II) complexes with paullone-modified ligands (**5** and **6**) in terms of suitability for further preclinical development as anticancer drugs.

Conflicts of interest

The authors declare no competing interest.

Acknowledgements

This work was supported by the Austrian Science Fund (FWF) *via* the Grant no. P31293-N37. EAE acknowledges the support by National Research, Development and Innovation Office-NKFIA through project FK 124240 and Ministry of Human Capacities, Hungary grant 20391-3/2018/FEKUSTRAT. The study was also supported by the project GINOP-2.3.2-15-2016-00038 of the University of Szeged. We thank Alexander Roller for the X-ray data collection. This work was also supported by the Science and Technology Assistance Agency under the contract no. APVV-15-0053 and SK-AT-2017-0017, and by the Slovak Grant Agency VEGA under contract no. 1/0416/17 and 1/0466/18. TR acknowledges the support of this work by National Institutes of Health *via* the grant P30 CA00874.

References

1 H. Blumberg, *U.S. Pat.*, US3790675A, 1974.
2 L. Toscano, G. Grisanti, G. Fioriello, E. Seghetti, A. Bianchetti, G. Bossoni and M. Riva, *J. Med. Chem.*, 1976, **19**, 208–213.
3 H. L. Koh, M. L. Go, T. I. Ngiam and J. W. Mak, *Eur. J. Med. Chem.*, 1994, **29**, 107–113.
4 X. Xie, T. Lemcke, R. Gussio, D. W. Zaharevitz, M. Leost, L. Meijer and C. Kunick, *Eur. J. Med. Chem.*, 2005, **40**, 655–661.
5 D. H.-C. Chou, N. E. Bodycombe, H. A. Carrinski, T. A. Lewis, P. A. Clemons, S. L. Schreiber and B. K. Wagner, *ACS Chem. Biol.*, 2010, **5**, 729–734.
6 J. Ryczak, M. Papini, A. Lader, A. Nasereddin, D. Kopelyanskiy, L. Preu, C. L. Jaffe and C. Kunick, *Eur. J. Med. Chem.*, 2013, **64**, 396–400.
7 C. Reichwald, O. Shimony, U. Dunkel, N. Sacerdoti-Sierra, C. L. Jaffe and C. Kunick, *J. Med. Chem.*, 2008, **51**, 659–665.
8 E. A. Sausville, D. Zaharevitz, R. Gussio, L. Meijer, M. Louarn-Leost, C. Kunick, R. Schultz, T. Lahusen, D. Headlee and S. Stinson, *Pharmacol. Ther.*, 1999, **82**, 285–292.
9 A. Huwe, R. Mazitschek and A. Giannis, *Angew. Chem., Int. Ed.*, 2003, **42**, 2122–2138.
10 C. Schultz, A. Link, M. Leost, D. W. Zaharevitz, R. Gussio, E. A. Sausville, L. Meijer and C. Kunick, *J. Med. Chem.*, 1999, **42**, 2909–2919.
11 A. Dobrov, V. B. Arion, N. Kandler, W. Ginzinger, M. A. Jakupec, A. Rufińska, N. Graf von Keyserlingk, M. Galanski, C. Kowol and B. K. Keppler, *Inorg. Chem.*, 2006, **45**, 1945–1950.
12 G. Mühlgassner, C. Bartel, W. F. Schmid, M. A. Jakupec, V. B. Arion and B. K. Keppler, *J. Inorg. Biochem.*, 2012, **116**, 180–187.
13 V. B. Arion, A. Dobrov, S. Göschl, M. A. Jakupec, B. K. Keppler and P. Rapta, *Chem. Commun.*, 2012, **48**, 8559–8561.
14 W. F. Schmid, R. O. John, V. B. Arion, M. A. Jakupec and B. K. Keppler, *Organometallics*, 2007, **26**, 6643–6652.
15 M. F. Primik, G. Mühlgassner, M. A. Jakupec, O. Zava, P. J. Dyson, V. B. Arion and B. K. Keppler, *Inorg. Chem.*, 2010, **49**, 302–311.
16 A. Dobrov, S. Göschl, M. A. Jakupec, A. Popović-Bijelić, A. Gräslund, P. Rapta and V. B. Arion, *Chem. Commun.*, 2013, **49**, 10007–10009.
17 W. F. Schmid, R. O. John, G. Muehlgassner, P. Heffeter, M. A. Jakupec, M. Galanski, W. Berger, V. B. Arion and B. K. Keppler, *J. Med. Chem.*, 2007, **50**, 6343–6355.
18 L. Keller, S. Beaumont, J.-M. Liu, S. Thoret, J. S. Bignon, J. Wdzieczak-Bakala, P. Dauban and R. H. Dodd, *J. Med. Chem.*, 2008, **51**, 3414–3421.
19 A. Putey, F. Popowycz, Q.-T. Do, P. Bernard, S. K. Talapatra, F. Kozielski, C. M. Galmarini and B. Joseph, *J. Med. Chem.*, 2009, **52**, 5916–5925.
20 A. Putey, L. Joucla, L. Picot, T. Besson and B. Joseph, *Tetrahedron*, 2007, **63**, 867–879.
21 V. Pons, S. Beaumont, M. E. Tran Huu Dau, B. I. Iorga and R. H. Dodd, *ACS Med. Chem. Lett.*, 2011, **2**, 565–570.
22 C. Marzano, M. Pellei, F. Tisato and C. Santini, *Anticancer Agents Med. Chem.*, 2009, **9**, 185–211.
23 F. Tisato, C. Marzano, M. Porchia, M. Pellei and C. Santini, *Med. Res. Rev.*, 2010, **30**, 708–749.
24 F. Bacher, O. Dömötör, A. Chugunova, N. V. Nagy, L. Filipović, S. Radulović, É. A. Enyedy and V. B. Arion, *Dalton Trans.*, 2015, **44**, 9071–9090.
25 M. F. Primik, S. Göschl, M. A. Jakupec, A. Roller, B. K. Keppler and V. B. Arion, *Inorg. Chem.*, 2010, **49**, 11084–11095.
26 L. wyffels, G. G. Muccioli, S. De Bruyne, L. Moerman, J. Sambre, D. M. Lambert and F. De Vos, *J. Med. Chem.*, 2009, **52**, 4613–4622.
27 V. Polshettiwar and M. P. Kaushik, *Tetrahedron Lett.*, 2004, **45**, 6255–6257.
28 *SAINT-Plus, version 8.32B and APEX2*, Bruker-Nonius AXS Inc., Madison, WI, 2016.
29 G. M. Sheldrick, *Acta Crystallogr., Sect. A: Found. Crystallogr.*, 2008, **64**, 112–122.
30 M. N. Burnett and G. K. Johnson, ORTEPIII. Report ORNL-6895, OAK Ridge National Laboratory, Tennessee, 1996.
31 H. M. N. H. Irving, M. G. Miles and L. D. Pettit, *Anal. Chim. Acta*, 1967, **38**, 475–488.
32 É. A. Enyedy, N. V. Nagy, É. Zsigó, C. R. Kowol, V. B. Arion, B. K. Keppler and T. Kiss, *Eur. J. Inorg. Chem.*, 2010, 1717–1728.

33 L. Zékány and I. Nagypál, *Computational Methods for the Determination of Stability Constants*, Plenum Press, New York, 1985.
34 É. A. Enyedy, D. Hollender and T. Kiss, *J. Pharm. Biomed. Anal.*, 2011, **54**, 1073–1081.
35 A. W. Addison, T. N. Rao, J. Reedijk, J. Van Rijn and G. C. Verschoor, *J. Chem. Soc., Dalton Trans.*, 1984, 1349–1356.
36 L. ChemAxon, *Instant J Chem/MarvinSketch*, ChemAxon Ltd., Budapest, Hungary, 2012.
37 M. Valko, C. J. Rhodes, J. Moncol, M. Izakovic and M. Mazur, *Chem.-Biol. Interact.*, 2006, **160**, 1–40.
38 M. Valko, H. Morris and M. T. D. Cronin, *Curr. Med. Chem.*, 2005, **12**, 1161–1208.
39 R. Evens, N. Beenaerts, T. Neyens, N. Witters, K. Smeets and T. Artois, *Sci. Rep.*, 2018, **8**, 3008.
40 R. J. Ferreira, M.-J. U. Ferreira and D. J. V. A. dos Santos, *J. Chem. Inf. Model.*, 2013, **53**, 1747–1760.
41 M. F. Primik, L. F. Filak and V. B. Arion, in *Organometallic Chemistry and Catalysis: The Silver/Gold Jubilee International Conference on Organometallic Chemistry Celebratory Book*, ed. A. J. L. Pombeiro, John Wiley & Sons, 1st edn, 2014, pp. 605–617.